PHYSICAL REVIEW B VOLUME 15, NUMBER 4 15 FEBRUARY 1977

Cluster model for the electronic structure of the Chevrel-phase compound $PbMo_6S_8$

L. F. Mattheiss and C. Y. Fong*
Bell Laboratories, Murray Hill, New Jersey 07974

(Received 28 September 1976)

A simplified model for the electronic structure of the Chevrel-phase compound $PbMo_6S_8$ is obtained by means of a tight-binding calculation for a cubic Mo_6S_8 cluster. The interaction parameters for this cluster calculation are derived from a tight-binding fit to the results of an *ab initio* augmented-plane-wave energy-band calculation for a hypothetical Mo_3S crystal with the Cu_3Au structure. It is found that the molecular-orbital states near the Mo_6S_8 Fermi level E_F consist of partially-filled nonbonding Mo $d_{x^2-y^2}$ -type orbitals. These results suggest the presence of narrow d-type conduction bands in compounds such as $PbMo_6S_8$ since bandwidths resulting from intercluster interactions are estimated to be small.

I. INTRODUCTION

The observation of high superconducting transition temperatures[1] (~15 °K) and high critical fields[2] (~500 kG) within the family of noncubic Chevrel-phase[3] compounds has generated considerable interest in their electronic structure. Among these materials, the nonstoichiometric compound $Pb_{0.92}Mo_6S_{7.5}$ has attracted the most attention since it has been found to have the highest superconducting transition temperature (15.2 °K).

X-ray studies by Marezio *et al.*[4] on a single-crystal $Pb_{0.92}Mo_6S_{7.5}$ sample yield a rhombohedral structure with space group $R\bar{3}$ and one formula unit per unit cell. This structure is most easily visualized as a distorted variation of the CsCl structure in which Pb replaces Cs at the origin and a cubic Mo_6S_8 cluster replaces Cl at $a(\frac{1}{2}, \frac{1}{2}, \frac{1}{2})$, where a is the length of the cube edge. The rhombohedral distortion involves a rotation of these Mo_6S_8 clusters about a $\langle 111 \rangle$ axis plus a slight noncubic deformation of the Mo_6S_8 complex.

Fisher *et al.*[2,5] have proposed that the Mo $4d$ electrons are responsible for the interesting superconducting properties of $PbMo_6S_8$. They suggest that, since the Mo_6S_8 clusters are well separated in space, one expects only a weak coupling between them. Consequently, they propose that these compounds can be regarded as "quasi-zero-dimensional" superconductors such that the electronic wave functions which are involved in superconductivity are essentially localized within a single Mo_6 octahedron.

The purpose of the present investigation is to provide a theoretical model for the electronic structure of $PbMo_6S_8$ based on the results of a molecular-orbital (MO) calculation for an idealized cubic Mo_6S_8 cluster. This Mo_6S_8 cluster calculation involves a total of 68 MO basis functions, each of which consists of a "linear-combination-of-atomic-orbitals" (LCAO) centered at the 14 atomic sites of the cluster. In particular, these LCAO-MO's involve symmetrized combinations of S $3s(8)$, S $3p(24)$, Mo $5s(6)$, and Mo $4d(30)$ atomic orbitals. The required energy and overlap interaction parameters for this Mo_6S_8 cluster calculation have been derived from an LCAO fit to an *ab initio* augmented-plane-wave (APW) energy-band calculation for hypothetical Mo_3S with the Cu_3Au structure.

There has been one previous study of the electronic structure of $PbMo_6S_8$ by Andersen *et al.*,[6] involving the atomic-sphere approximation to the Korringa-Kohn-Rostoker and linear combination of muffin-tin orbitals methods. Because of the complexity of the $PbMo_6S_8$ crystal structure, they limited their study to two approximate model calculations. First, they determined the 30 canonical $4d$ bands of the Mo_6 cluster. Then, they included the effects of hybridization (with the Mo $5s$ orbitals) and covalent mixing (with the S $3p$ states) and carried out calculations for a Mo_6S_{14} cluster. This corresponds to the Mo_6S_8 cluster of the present investigation, with the addition of six nearest S atoms from neighboring Mo_6S_8 clusters.

The results of these two investigations agree in predicting that the electrons near the Fermi energy E_F have predominantly $d_{x^2-y^2}$ symmetry in these Chevrel-phase compounds. However, there appear to be some differences in the results of the two calculations concerning the relative ordering of states near E_F. In particular, the present calculations predict that the MO level at E_F is threefold degenerate and has Γ_{25} symmetry, whereas Andersen *et al.*[6] obtain a doubly-degenerate level with Γ_{12} symmetry.

A brief discussion of the $PbMo_6S_8$ crystal structure is presented in Sec. II. The details of the APW calculations for Mo_3S and the evaluation of the LCAO parameters from these energy-band results is discussed in Sec. III. In Sec. IV, we

present the results of both the APW calculations for Mo_3S and the LCAO-MO calculation for Mo_6S_8. Section V includes a discussion of these results, particularly their applicability to the $PbMo_6S_8$ crystal.

II. CRYSTAL STRUCTURE

The crystal structure of $PbMo_6S_8$ has been determined by Marezio *et al.*,[4] who identify its space group as $C_{3i}^2(R\bar{3})$. This symmorphic space group is associated with the trigonal system, and has a rhombohedral Bravais lattice with primitive vectors $|\vec{t}_1| = |\vec{t}_2| = |\vec{t}_3| = 6.551$ Å making equal angles α with each other, where α is very nearly 90° (89.33°).

A schematic representation of the $PbMo_6S_8$ crystal structure is shown in Fig. 1. It consists basically of a CsCl-type structure in which the Cs atoms are replaced by Pb while the Cl atoms are replaced by a distorted Mo_6S_8 cluster. This Mo_6S_8 cluster consists of a warped subcube with Mo atoms near the face centers and S atoms close to the corners. A projection of an idealized cubic version of this structure along a cube edge is shown in Fig. 1(a). Here, the cubic cell dimension $a \approx 6.55$ Å while that of the Mo_6S_8 subcube $b \approx 3.83$ Å. In this idealized geometry, the intracluster Mo-Mo separation $b/\sqrt{2}$ (2.71 Å) is comparable with the intercluster bond distance b-a (2.72 Å).

A projection of the actual distorted $PbMo_6S_8$ structure[4] along a rhombohedral axis is shown in Fig. 1(b). The distortion consists primarily of a rotation of the Mo_6S_8 subcubes along a ⟨111⟩ axis plus additional deviations from cubic symmetry within the Mo_6S_8 clusters. An important feature of this distortion is that the diameter of the Mo_6 octahedron (~3.83 Å) is significantly larger than the edge of the S_8 subcube (~3.46 Å). As a result,

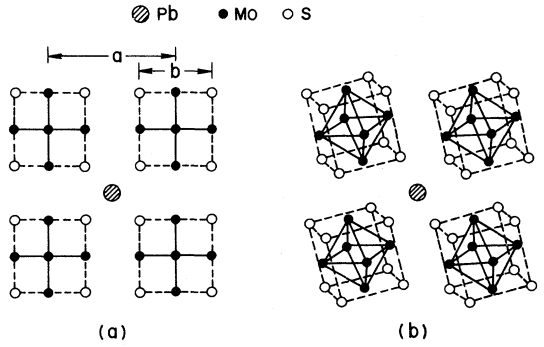

FIG. 1. (a) Projection of an idealized cubic modification of $PbMo_6S_8$ along a cube axis; (b) projection of rhombohedral $PbMo_6S_8$ down a rhombohedral a axis.

the nearest-neighbor Mo-Mo intracluster bond distances are 2.67 and 2.74 Å, respectively, while the corresponding Mo-S distances are somewhat smaller and range from 2.39 to 2.51 Å.

A more obvious result of this rhombohedral distortion is that of reducing the strength of Mo-Mo and S-S bonding interactions between neighboring Mo_6S_8 complexes. In the undistorted case of Fig. 1(a), the intercluster Mo-Mo bond length is 2.72 Å; this is increased to 3.27 Å in the distorted geometry of Fig. 1(b). On the other hand, the distortion tends to optimize the formation of intercluster S-Mo $3p$-$4d$ bonds. This bond distance, which is originally 3.83 Å in the undistorted geometry of Fig. 1(a), is reduced by the distortion to 2.57 Å in Fig. 1(b).

The eight S atoms in the unit cell are subdivided into two types. Two sulfurs are at positions with C_3 site symmetry; the remaining six S atoms are at general positions in the cell, where the point group includes only the identity operation. The six Mo atoms are also situated at general positions in the cell; the Pb atom is at the origin, where the site symmetry is C_{3i}.

III. DETAILS OF THE CALCULATION

The direct application of standard energy-band methods to determine the electronic structure of $PbMo_6S_8$ is complicated by the low symmetry of the structure (C_{3i}^2) as well as the large number of atoms in the unit cell (15). It is estimated that an APW calculation for $PbMo_6S_8$ would require roughly 600 basis functions in order to obtain energy eigenvalues converged to approximately 0.002 Ry. Furthermore, the low symmetry of the structure precludes the possibility of reducing the size of the APW matrix appreciably, even at symmetry points in the Brillouin zone.

As a result of these difficulties, we have limited the scope of this investigation to that of studying the MO wave functions and energy levels of an idealized cubic Mo_6S_8 cluster. The LCAO parameters for this cluster calculation have been determined by means of a tight-binding fit to the APW results for a hypothetical Mo_3S crystal with the Cu_3Au structure. The unit cell for this structure is shown in Fig. 2(a), where the three Mo atoms are at the face centers and the S atom is located at the corner of the simple-cubic unit cell. It is clear that this unit cell has the same basic symmetry as the Mo_6S_8 clusters in Fig. 1; the latter do not share atoms on the cube faces with neighboring clusters, thereby changing the composition from Mo_3S to Mo_6S_8.

In the APW calculation for cubic Mo_3S, we have used a lattice parameter b equal to $\sqrt{2}$ times the

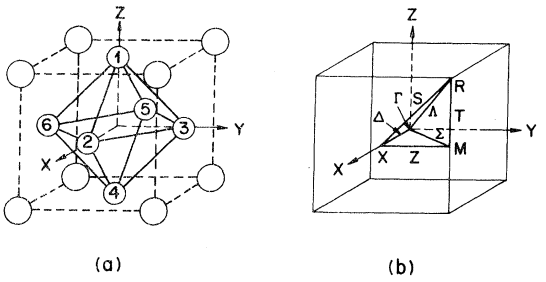

FIG. 2. (a) Unit cell of Mo_3S with the Cu_3Au structure, having Mo atoms at the face centers and a S atom at each corner; (b) Brillouin zone for the simple cubic Bravais lattice.

average Mo-Mo separation within the Mo_6S_8 cluster of the $PbMo_6S_8$ crystal, namely $b = 3.79$ Å.[7] The methods used to set up the crystal potential are analogous to those discussed in Ref. 8. This *ad hoc* potential is derived from Herman-Skillman[9] atomic charge densities for Mo and S with electronic configurations $5s^1 4d^5$ and $3s^2 3p^4$, respectively. The muffin-tin radii for the Mo and S spheres are chosen so that $R_{Mo} = R_S$. Their magnitudes are such that neighboring spheres touch along the nearest-neighbor Mo-S and Mo-Mo bond directions.

The APW calculations for hypothetical Mo_3S have been carried out at ten points in the simple-cubic Brillouin zone shown in Fig. 2(b). These include the four symmetry points (Γ, X, M, R) and the midpoints of the six symmetry lines ($\Delta, \Sigma, \Lambda, Z, S, T$). Approximately 150–160 APW basis functions have been included in these calculations and convergence errors are estimated to be in the 0.002-Ry range. The utilization of standard symmetrization techniques allows one to factor the APW matrices so that their maximum dimension is 54×54.

The Slater-Koster LCAO interpolation method[10] has been applied to fit the results of these APW calculations at symmetry points and along symmetry lines of the Brillouin zone. This LCAO model involves a total of 22 basis functions. These include 18 Bloch sums formed from the Mo $5s$ and $4d$ orbitals (which number 3 and 15, respectively) as well as four tight-binding functions derived from the S $3s$ and $3p$ atomic states. Bloch sums derived from the Mo $5p$ manifold have omitted in this treatment.

The point symmetries at the Mo and S sites in the hypothetical Mo_3S crystal are D_{4h} and O_h, respectively. In setting up Bloch sums, it is useful to utilize orbitals which transform irreducibly under the appropriate point-group operations. At the Mo site labeled 1 in Fig. 2(a), the appropriate $4d$ orbitals are $d_{xy}(X_3)$, d_{yz}, $d_{xz}(X_5)$, $d_{3z^2-r^2}(X_1)$, and $d_{x^2-y^2}(X_2)$, where the labels in parentheses indicate their transformation properties according to the notation of Bouckaert *et al.*[11] The corresponding orbitals at sites 2 and 3 in Fig. 2(a) are obtained by cyclically permuting the coordinates (x, y, z). Thus, the orbitals at sites 2 and 3 which are equivalent to $d_{x^2-y^2}$ at site 1 are $d_{y^2-z^2}$ and $d_{z^2-x^2}$, respectively. Throughout the remainder of this paper, references to the entire set of equivalent orbitals (for example, $d_{x^2-y^2}$, $d_{y^2-z^2}$, $d_{z^2-x^2}$) are designated by enclosing the prototype site 1 orbital in braces $\{d_{x^2-y^2}\}$.

As a result of the D_{4h} point-group symmetry at the Mo sites, the Mo $4d$ bands can be subdivided into four subbands, each of which possesses a distinct orbital energy in the LCAO scheme. These orbital energies are labeled $E_d(xy)$, $E_d(yz, zx)$, $E_d(x^2 - y^2)$, and $E_d(3z^2 - r^2)$. A single orbital energy is appropriate for describing either the S $3s$ or $3p$ manifolds, since the S-atom point symmetry is O_h.

In setting up our LCAO interpolation scheme for the Mo_3S structure, we include the appropriate nearest- and second-neighbor interactions along both the $(\frac{1}{2}b, \frac{1}{2}b, 0)$ and $(b, 0, 0)$ bond axes. These interactions reduce to a total of 26 independent tight-binding parameters in the two-center approximation, assuming orthogonalized orbitals at each atomic site (LCOAO model). An improved fit is obtained by including nearest-neighbor orbital overlap between each pair of unlike orbitals (LCAO model). This increases the number of LCOAO two-center parameters by 6, leading to a total of 32 for the LCAO model.

Using a nonlinear least-squares-fitting procedure that has been described previously,[12] the LCOAO-LCAO parameters for hypothetical Mo_3S have been determined from the APW results at the ten points in the Brillouin zone. The task of identifying APW eigenvalues and matching them with the appropriate tight-binding orbitals requires a minor extension of the results tabulated in Table I of both Refs. 8(a) and 8(b). In the present application, the LCOAO-LCAO model has been applied to fit a total of 220 APW eigenvalues (neglecting symmetry-induced degeneracies) by means of 26 or 32 parameters. With reasonable starting values, the fitting procedure converged within 6–8 iterations with final rms errors in the range 0.03–0.05 Ry.

This LCOAO-LCAO model is readily extended to treat the isolated Mo_6S_8 cluster of Fig. 2(a). Here, the number of Mo atoms increases from 3 to 6 since the pairs of atoms labeled 1 and 4, 2 and 5, and 3 and 6 in Fig. 2(a) are no longer equivalent because of translational symmetry. The

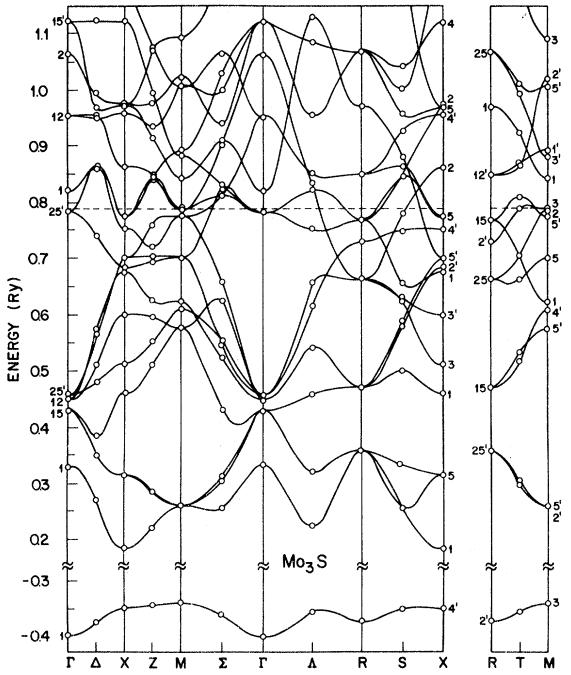

FIG. 3. APW energy-band results for hypothetical Mo_3S.

same is true for the eight S atoms at the cube corners. As a result, the LCOAO-LCAO matrix for the Mo_6S_8 cluster has dimensions 68×68 when Mo $5s$, Mo $4d$, S $3s$, and S $3p$ atomic orbitals are included in the set of MO basis functions.

The point symmetries at the Mo(C_{4v}) and S(C_{3v}) sites of the Mo_6S_8 cluster are reduced from those of the Mo_3S crystal (D_{4h} and O_h, respectively). The C_{4v} symmetry again subdivides the Mo $4d$ orbitals into four subgroups, including $\{d_{xy}\}(\Delta_2')$, $\{d_{yz}, d_{xz}\}(\Delta_5)$, $\{d_{3z^2-r^2}\}(\Delta_1)$, and $\{d_{x^2-y^2}\}(\Delta_2)$. This leads to the same number of d-orbital energies as the Mo_3S crystal. The C_{3v} symmetry at a S site separates the $3p$ states into two sublevels, $\{p_{x+y+z}\}(\Lambda_1)$ and $\{p_{2x-y-z}, p_{y-z}\}(\Lambda_3)$. These sublevels can have independent orbital energies in the Mo_6S_8 cluster, though these refinements are neglected in the present simplified treatment. For simplicity, we also neglect the effects for spin-orbit coupling in this calculation. It is expected that level splittings and shifts resulting from the noncubic distortions of the Mo_6S_8 cluster will be larger than those caused by spin-orbit coupling.

IV. RESULTS

The APW energy-band results for hypothetical Mo_3S are plotted in Fig. 3 along the six symmetry lines of the Brillouin zone. The zero of energy for these bands coincides with the average value of the potential in the region between the APW spheres, $V_0 = -1.384$ Ry. The approximate Fermi energy, which is indicated by the dashed horizontal line, falls near the middle of the 15 Mo $4d$ bands. Generally speaking, these Mo $4d$ bands span an energy range that extends from about 0.45 to 1.25 Ry. Located just below the Mo $4d$ bands (in the energy range 0.18–0.43 Ry) are the S $3p$ bands and the bottom of the Mo $5s$ band. The lowest band shown near the bottom of the figure is that of the S $3s$ states.

States associated with the Mo $5s$ bands extend to energies as high as 1.7 Ry. The energies of these higher bands are fit only approximately by means of the LCAO interpolation scheme. In order to minimize the influence of these higher bands on the overall quality of the LCAO fit, we have arbitrarily assigned these higher bands a reduced weight (0.1 vs 1) in the LCAO fitting procedure. The difficulty in fitting these higher unoccupied bands arises partially from the omission of the Mo $5p$ orbitals from our LCAO model. For example, there are two states shown in the upper portion of Fig. 3 (R_1 and M_3) which are omitted from the LCAO fitting procedure; their symmetry indicates that they represent the lowest states of the Mo $5p$ bands.

The parameters that are obtained from the LCOAO-LCAO fits to the APW results of Fig. 3 are listed in Table I. In each case, the rms error includes the reduced weighting of the upper Mo $5s$ bands. These states are also excluded from the maximum error that is quoted for each fit.

The use of these tight-binding two-center parameters in the LCOAO-LCAO Hamiltonian-overlap matrices permits us to predict the MO energy-level scheme for the Mo_6S_8 cluster. The results of these calculations are shown in Fig. 4. These results are also plotted relative to the muffin-tin constant, $V_0 = -1.384$ Ry. The results in columns (a) and (b) are derived from the LCOAO and LCAO models, respectively. In both cases, the symmetry of the MO's is classified according to the irreducible representations of the O_h point group.[11] The detailed manner in which the MO's formed from the Mo $4d$, Mo $5s$, S $3s$, and S $3p$ orbitals are decomposed into the various symmetry types is summarized in Table II.

It is found that the 68 eigenvalues of the Mo_6S_8 cluster Hamiltonian combine to produce a total of 30 distinct MO energy levels, including eight that are nondegenerate ($4\Gamma_1, 1\Gamma_2, 3\Gamma_{2'}$), six that are doubly degenerate ($4\Gamma_{12}, 2\Gamma_{12'}$), and 16 that are triply degenerate ($6\Gamma_{15}, 3\Gamma_{25}, 2\Gamma_{15'}, 5\Gamma_{25'}$). These 30 MO levels can be separated into four distinct subgroups. The lowest group of 4 MO levels in Figs. 4(a) and 4(b) correspond to the S $3s$ states. The

TABLE I. LCOAO and LCAO two-center parameters (Ry), as derived from APW results for Mo_3S. The Mo 5s and S 3s orbitals are labeled S and s, respectively. The subscripts 1 and 2 correspond to the nearest- and second-neighbor bond directions $\vec{r}_1 = b(\frac{1}{2}, \frac{1}{2}, 0)$ and $\vec{r}_2 = b(1, 0, 0)$, respectively. Square brackets denote overlap integrals.

Parameter	LCOAO	LCAO	Parameter	LCOAO	LCAO
E_s	−0.2750	−0.3121	$(dd\pi)_2$	−0.0033	0.0087
$(ss\sigma)_2$	−0.0135	−0.0076	$(dd\delta)_2$	0.0035	0.0021
E_p	0.4420	0.3932	$(sp\sigma)_2$	0.0252	−0.0236
$(pp\sigma)_2$	0.0141	0.0166	$(sS\sigma)_1$	−0.0041	−0.0089
$(pp\pi)_2$	0.0019	0.0014	$(sd\sigma)_1$	−0.0706	−0.0692
E_S	1.0496	0.8853	$(pS\sigma)_1$	−0.0951	−0.0287
$(SS\sigma)_1$	−0.0367	−0.0515	$(pd\sigma)_1$	−0.0989	−0.0142
$(SS\sigma)_2$	−0.0003	0.0161	$(pd\pi)_1$	0.0224	0.0390
$E_d(xy)$	0.7544	0.6892	$(Sd\sigma)_1$	−0.0724	0.0499
$E_d(yz, zx)$	0.7865	0.7524	$(Sd\sigma)_2$	0.0015	0.0046
$E_d(x^2-y^2)$	0.7451	0.7250	$[sS\sigma]_1$	···	0.0526
$E_d(3z^2-r^2)$	0.7270	0.7150	$[sd\sigma]_1$	···	0.0576
$(dd\sigma)_1$	−0.0998	−0.0972	$[pS\sigma]_1$	···	0.0838
$(dd\pi)_1$	0.0583	0.0715	$[pd\sigma]_1$	···	0.1421
$(dd\delta)_1$	−0.0083	−0.0206	$[pd\pi]_1$	···	−0.0179
$(dd\sigma)_2$	−0.0128	−0.0194	$[Sd\sigma]_1$	···	0.1407
rms error	0.0463	0.0284	max. error	0.1337	0.0643

next group of ten levels evolve from the S 3p states. These are separated by a small gap from the 13 Mo 4d levels. Finally, the highest three levels involve the Mo 5s states.

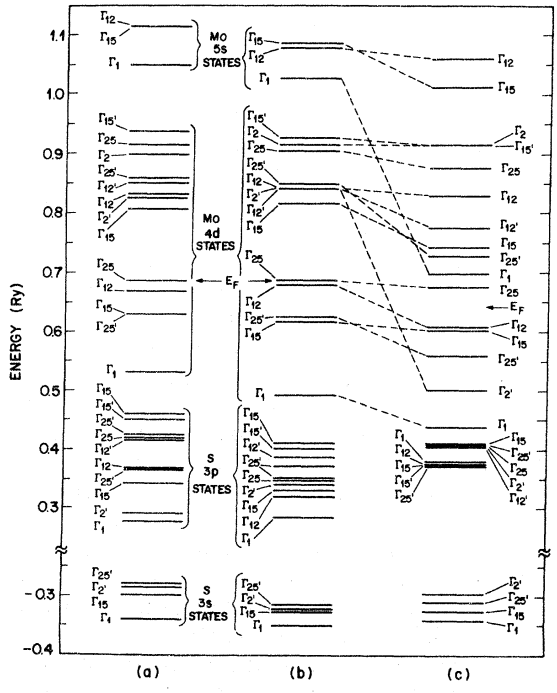

FIG. 4. (a) LCOAO energy levels for the Mo_6S_8 cluster; (b) corresponding results for the LCAO model; and (c) LCAO levels with all Mo-S covalency-overlap parameters set equal to zero.

Neglecting core states, the Mo_6S_8 cluster contains a total of 84 electrons. By filling each MO level with the appropriate number of spin-up and spin-down electrons, it is found that the last two electrons partially fill the triply-degenerate (neglecting spin) Γ_{25} state, whose energy is approximately 0.69 Ry in Figs. 4(a) and (b). Thus, this MO calculation predicts "metallic" properties for the Mo_6S_8 cluster.

Of particular interest are the MO states near E_F. Both the LCOAO and LCAO models predict an ordering of levels such that a Γ_{25} state at E_F is partially filled by two electrons. However, as discussed presently in Sec. V, the energy separation between this Γ_{25} level and the lower Γ_{12} state (0.01–0.02 Ry) is probably less than the over-

TABLE II. Symmetry of MO's formed from Mo 5s(S), Mo 4d(d_{xy}; d_{yz}, d_{zx}; $d_{x^2-y^2}$; $d_{3z^2-r^2}$)S 3s(s), and S 3p(p_x, p_y, p_z) orbitals of the Mo_6S_8 cluster.

Atom	Orbitals	MO Symmetry
Mo	$\{S\}$	$\Gamma_1, \Gamma_{12}, \Gamma_{15}$
	$\{d_{xy}\}$	$\Gamma_{2'}, \Gamma_{12'}, \Gamma_{25'}$
	$\{d_{yz}, d_{zx}\}$	$\Gamma_{15'}, \Gamma_{25'}, \Gamma_{15}, \Gamma_{25}$
	$\{d_{x^2-y^2}\}$	$\Gamma_2, \Gamma_{12}, \Gamma_{25}$
	$\{d_{3z^2-r^2}\}$	$\Gamma_1, \Gamma_{12}, \Gamma_{15}$
S	$\{s\}$	$\Gamma_1, \Gamma_{2'}, \Gamma_{25'}, \Gamma_{15}$
	$\{p_x, p_y, p_z\}$	$\Gamma_1, \Gamma_{2'}, \Gamma_{12}, \Gamma_{12'}, 2\Gamma_{25'}, \Gamma_{15'}, \Gamma_{25}, 2\Gamma_{15}$

all accuracy of the present calculation. Consequently, we do not regard this ordering of levels as a firm prediction of the model.

Perhaps the most interesting result of these tight-binding calculations for the Mo_6S_8 cluster is the presence of a distinct gap in the distribution of MO levels above E_F. This 0.11–0.13-Ry gap separates the 30 Mo $4d$ MO levels into a lower nearly-filled subgroup of 12 states and an upper unoccupied manifold of 18 levels. This separation of the 30 d levels into two subgroups with two and three states/Mo atom, respectively, is reminiscent of the ligand-field splitting of a fivefold-degenerate d level into doubly-degenerate (e_g) and triply-degenerate (t_{2g}) levels in a cubic environment. In the present geometry, this gap can be regarded as separating the nearly-filled nonbonding Mo $4d$ MO's from the upper unoccupied "antibonding" states. The "bonding" counterparts of these states, which are labeled S $3s$ and $3p$ states in Figs. 4(a) and 4(b), are responsible for the structural stability of this molecular complex.

To illustrate the effect of these Mo-S bonds on the distribution of MO levels for the Mo_6S_8 cluster, we plot the LCAO-MO levels for the noninteracting Mo_6 and S_8 clusters in Fig. 4(c). These results are obtained by setting all Mo-S covalency-overlap parameters equal to zero in the LCAO Hamiltonian and overlap matrices. It is found that the omission of these Mo-S interactions reduces the energy spread of the S $3p$ levels by about a factor of 3, but produces a slight increase in that of the $3s$ levels. On the other hand, the Mo_6 octahedral cluster produces a rather uniform distribution of $4d$ levels, with little change in their over-all width. There is a significant reduction in the energy of the lowest Mo $5s$ level (Γ_1), which now lies near the middle of the $4d$ levels, thereby producing an overlap in energy of the $5s$ and $4d$ manifolds.

Among the Mo $4d$ levels, the largest energy shift is that of the MO with $\Gamma_{2'}$ symmetry, which now lies below E_F in Fig. 4(c). The filling of this state lowers E_F to the midpoint of the Γ_{12}-Γ_{25} energy gap. The reason for this large shift in the energy of the $\Gamma_{2'}$ level is readily identified by examining of the MO wave function for this state, as discussed in Sec. V.

V. DISCUSSION

Since the present tight-binding model involves an extrapolation from the energy bands of the Mo_3S crystal to those of the Mo_6S_8 cluster, it is gratifying to find that the principal features of these cluster results are reasonably independent of the details of the interpolation scheme. According to Figs. 4(a) and 4(b), the over-all distribution of MO levels predicted by the LCOAO and LCAO models is quite similar. The main differences involve the over-all "bandwidths" spanned by the S $3s$ and $3p$ levels. With few exceptions, the same ordering of MO levels is predicted by both models near E_F.

In this regard, it is worth mentioning that a complete APW-LCOAO calculation has been carried through for Mo_3S with a slightly larger (3.4%) lattice constant. This calculation yields essentially the same distribution of MO levels for the Mo_6S_8 cluster as shown in Fig. 4(a), but with slightly reduced "bandwidths."

In order to better understand the distribution of MO levels near E_F in Fig. 4, it is useful to examine the orbital content of these states. These results, for the LCAO model of Fig. 4(b), are summarized in Table III. The entries in this table represent a sum of the squares of the appropriate eigenvector coefficients for the various Mo $5s$ and $4d$ Bloch sums, each of which has been orthogonalized by the Löwdin technique.[13]

The difference between 1 and the sum of entries in any given row of Table III is a measure of the covalent mixing of that state with the S $3s$ and $3p$ orbitals. Obviously, these quantities correlate with the level shifts that occur between the results shown in Figs. 4(b) and 4(c) when the Mo-S interactions are switched off. In particular, the largest covalent mixing (32.3%) and energy shift (– 0.34 Ry) occurs for the $\Gamma_{2'}$ state within the Mo $4d$ manifold. This is readily understood in terms of the results in Table III. It is found that this state consists primarily of $\{d_{xy}\}$ orbitals whose charge distribution is concentrated along the Mo-S bond directions, thereby enhancing the formation of strong Mo-S bonds.

Of particular interest is the orbital content of the Γ_{25} Γ_{12} states near E_F in Fig. 4(b). Both states involve primarily the nonbonding $\{d_{x^2-y^2}\}$ orbitals, though the latter (Γ_{12}) interacts more strongly with the S $3p$ orbitals. The energy separation and relative ordering of these two states clearly depends on an accurate treatment of both hybridization and covalency effects. As a result, we do not regard the Γ_{25}-Γ_{12} ordering of levels as a firm prediction of this calculation. In a sense, this issue may be regarded as being somewhat academic since the noncubic distortion of the Mo_6S_8 cluster could very well split or shift either level by energies greater than their 0.01–0.02-Ry separation.

As discussed in Sec. II, the distortion of the Mo_6S_8 cluster in $PbMo_6S_8$ can be separated into "cubic" and "noncubic" components. The former consists of a 9% reduction in the dimension of the S_8 subcube relative to the diameter of the Mo_6

TABLE III. Analysis of LCAO-MO cluster wave functions near E_F in terms of their fractional Mo 5s(S) and 4d(d_{xy}, d_{yz}, etc.) orbital content.

State	Energy (Ry)	{S}	$\{d_{xy}\}$	$\{d_{yz}, d_{zx}\}$	$\{d_{x^2-y^2}\}$	$\{d_{3z^2-r^2}\}$
$\Gamma_{15'}$	0.929	•••	•••	0.970	•••	•••
Γ_2	0.918	•••	•••	•••	1.000	•••
Γ_{25}	0.907	•••	•••	0.698	0.256	•••
$\Gamma_{25'}$	0.850	•••	0.833	0.021	•••	•••
Γ_{12}	0.844	0.001	•••	•••	0.016	0.970
$\Gamma_{2'}$	0.842	•••	0.677	•••	•••	•••
$\Gamma_{12'}$	0.841	•••	0.917	•••	•••	•••
Γ_{15}	0.818	0.000	•••	0.192	•••	0.737
Γ_{25}	0.689(E_F)	•••	•••	0.289	0.690	•••
Γ_{12}	0.681	0.014	•••	•••	0.825	0.004
$\Gamma_{25'}$	0.627	•••	0.000	0.886	•••	•••
Γ_{15}	0.618	0.101	•••	0.657	•••	0.210
Γ_1	0.495	0.247	•••	•••	•••	0.698

octahedron such that the Mo and S atoms are no longer coplanar in the cube faces of Fig. 2(a). This preserves the overall cubic symmetry of the Mo_6S_8 cluster and causes the original MO levels to be shifted but not split. On the other hand, the "noncubic" component distorts both the Mo_6 octahedron and the S_8 subcube. It changes two of the three Mo-Mo-Mo bond angles from 60° to 58.42° and 60.79°, respectively, and the three S-S-S bond angles from 90° to 88.8°, 90.1°, and 92.2°, respectively.[4] The "noncubic" distortion removes all symmetry-induced degeneracies of the cubic Mo_6S_8 cluster.

We have applied the present LCAO model to estimate the shifts in the MO energy levels that are caused by the "cubic" component of the distortion. In the two-center approximation, this involves a modification of the direction cosines (l, m, n) to describe the S-Mo(s-d, p-d, etc.) interaction parameters[10] in a nonplanar geometry. Initially, we assume no change in the values of the two-center parameters listed in Table I. The results of this calculation are shown in Fig. 5(b). For comparison, the original LCAO results of Fig. 4(b) are reproduced in Fig. 5(a); dashed lines are used to connect MO states with the same symmetry.

In general, the energy shifts between the MO levels in Figs. 5(a) and 5(b) are quite small. The largest changes (~0.04 Ry) involve the MO levels with Γ_1 and $\Gamma_{2'}$ symmetry. This is not unexpected since these levels experience the largest energy shifts in Figs. 4(b) and 4(c) when the S-Mo interactions are switched off entirely.

An important feature of this "cubic" distortion is that it reduces both the S-Mo and S-S bond distances by 9%. This should cause an increase in the strength of both the S-Mo and S-S two-center interaction parameters. We estimate this effect by increasing the appropriate LCAO parameters in Table I by 10%. The resulting LCAO-MO levels are shown in Fig. 5(c). It is seen that these changes in bond angles and bond strengths tend to cancel one another and the final distribution of MO

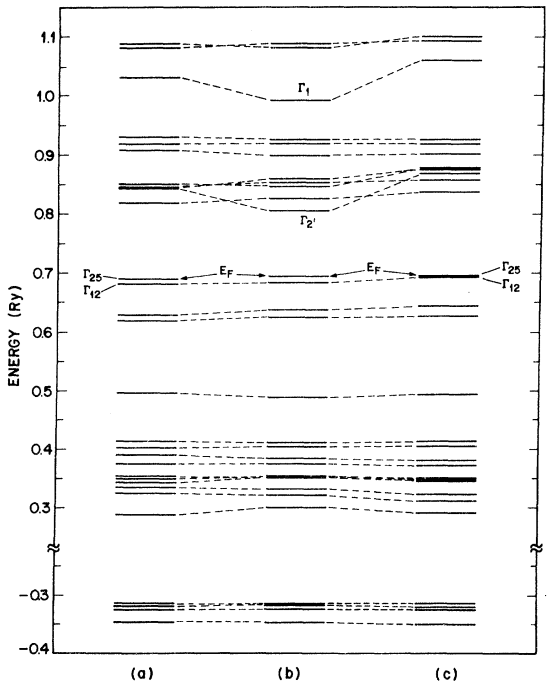

FIG. 5. (a) LCAO energy levels for the Mo_6S_8 cluster; (b) corresponding LCAO results with the S_8 subcube dimension reduced by 9% and two-center parameters unchanged; and (c) LCAO results with reduced (9%) S_8 subcube dimension and increased (10%) S-S and S-Mo two-center parameters.

energy levels is essentially equivalent to that shown in Fig. 5(a).

Let us now consider the relationship between these cubic Mo_6S_8 cluster results and the energy bands for rhombohedral $PbMo_6S_8$. The rhombohedral distortion will remove all the degeneracies of the cubic Mo_6S_8 cluster levels and introduce splittings which we estimate to be 0.02–0.03 Ry. The inclusion of intercluster interactions will broaden these levels into bands. An important question that remains concerns the role of the Pb atom in this system.

According to Marezio *et al.*,[4] each Pb atom in the $PbMo_6S_8$ crystal is surrounded by a distorted cube of eight S atoms at distances ranging from 2.79 to 3.12 Å. The Pb-Mo separation is even larger (4.23 Å). The Pb 6*s* electrons are tightly bound because of relativistic effects. According to the atomic results of Herman and Skillman[9] (including the Darwin and mass-velocity corrections), the Pb 6*s* atomic level lies approximately midway between the S 3*s* and 3*p* atomic states. Therefore, we expect the Pb 6*s* orbitals to form a fairly narrow band that is located well below E_F in $PbMo_6S_8$, centered near 0.1–0.2 Ry on the energy scale of Fig. 4. A similar analysis for the Pb 6*p* bands places their center of gravity well above E_F, near the Mo 5*s* states in Fig. 4(b). This suggests that Pb is divalent in $PbMo_6S_8$ and transfers its two 6*p* electrons to the Mo 4*d* bands. The effect of Pb-Mo interactions on the energy-band states near E_F is expected to be negligible.

The transfer of the two Pb electrons to the Mo 4*d* bands leaves two holes in the five $\{d_{x^2-y^2}\}$ bands near E_F that evolve from the Γ_{25} and Γ_{12} MO states. It is expected that the width of these subbands near E_F will be quite small because the intercluster coupling of the predominant $\{d_{x^2-y^2}\}$ orbitals is weak. This implies a large density of states near E_F, which is usually favorable for high-temperature superconductivity.

Andersen *et al.*[6] have proposed a model to explain the rotation of the Mo_6S_8 clusters in rhombohedral $PbMo_6S_8$ and related compounds in terms of intercluster coupling of the $\{d_{x^2-y^2}\}$ orbitals. In our view, this model overemphasizes the importance of electrons near E_F in explaining this phenomenon. It also depends on the relatively weak intercluster coupling of the $\{d_{x^2-y^2}\}$ orbitals. These intercluster interactions involve a $(dd\delta)$ bond in the undistorted geometry of Fig. 1(a). As the Mo_6S_8 subcubes are gradually rotated to form the rhombohedral $PbMo_6S_8$ structure of Fig. 1(b), these intercluster matrix elements are augmented by the larger $(dd\pi)$ and $(dd\sigma)$ components, but the Mo-Mo bond distance is simultaneously increased from 2.73 to 3.27 Å. Figure 1 of Ref. 6 indicates that the magnitude of this interaction never exceeds $|(dd\delta)|$. Since the intracluster and intercluster Mo-Mo bond distances are nearly equal in the undistorted geometry of Fig. 1(a), we can estimate this interaction [using $(dd\delta)_1$ of Table I] to be 0.01–0.02 Ry.

We suggest a possible alternate explanation of this distortion. Namely, we propose that the rotation of the Mo_6S_8 subcubes is such as to optimize the formation of $(pd\sigma)$ bonds between the Mo $\{d_{3z^2-r^2}\}$ orbitals of one cluster and the appropriate S 3*p* orbital on the neighboring one. Since this intercluster Mo-S bond distance (2.57 Å) is comparable to the average intracluster value (2.44 Å), we can again utilize the LCOAO-LCAO parameters of Table I $[E_p, E_d(3z^2-r^2), (pd\sigma)_1, [pd\sigma]_1]$ to estimate the energy shifts caused by these intercluster 3*p*-4*d* interactions. These calculations predict shifts of ± 0.03 Ry for the LCOAO model and values of − 0.014 and + 0.05 Ry for the LCAO model.

These calculated energy shifts provide realistic estimates of the bandwidths that are caused by intercluster *p*-*d* and *d*-*d* interactions in $PbMo_6S_8$. On the basis of these estimates, we conclude that the MO levels of Figs. 4 and 5 provide a reasonably accurate picture of the electronic structure of $PbMo_6S_8$. It is predicted that E_F lies near the top of a fairly narrow (~0.05 Ry) complex of 5 $\{d_{x^2-y^2}\}$ subbands. It also seems likely that these partially filled subbands are separated by a 1–2-eV gap from the next group of "antibonding" 4*d* bands. Because of their strong interaction with the S 3*s*-3*p* states, the Mo 5*s*-5*p* bands are expected to remain well above E_F, perhaps overlapping the top of the Mo 4*d* bands. It is worth noting that these gross features are not unlike those obtained previously in similar calculations for another anisotropic Mo-S compound, namely the layer compound $2H$-MoS_2.[14]

ACKNOWLEDGMENTS

We would like to thank P. W. Anderson for bringing the subject matter of this investigation to our attention. We are also grateful to C. M. Varma for several interesting discussions.

*On leave from the Dept. of Physics, University of California, Davis, Calif. 95616.

[1]B. T. Matthias, M. Marezio, E. Corenzwit, A. S. Cooper, and H. E. Barz, Science 175, 1465 (1972).

[2]Ø. Fisher, H. Jones, G. Bongi, M. Sergent, and R. Chevrel, J. Phys. C 7, L450 (1974).

[3]R. Chevrel, M. Sergent, and J. Pringent, J. Solid State Chem. 3, 515 (1971).
[4]M. Marezio, P. D. Dernier, J. P. Remeika, E. Corenzwit, and B. T. Matthias, Mater. Res. Bull. 8, 657 (1973).
[5]Ø. Fisher, in *Proceedings of the Fourteenth International Conference on Low Temperature Physics*, edited by M. Krusius and M. Vuorio (North-Holland, Amsterdam, 1975), Vol. 5, p. 172.
[6]O. K. Andersen, W. Klose, and H. Nohl (unpublished).
[7]Because of a misprint in Table 2 of Ref. 4, our value of b is slightly smaller than that (3.83Å) obtained using the correct average Mo-Mo separation. This small difference is not expected to affect our results in any significant way.
[8]L. F. Mattheiss, Phys. Rev. 181, 987 (1969); and Phys. Rev. B 2, 3918 (1970).
[9]F. Herman and S. Skillman, *Atomic Structure Calculations* (Prentice Hall, Englewood Cliffs, N. J., 1963).
[10]J. C. Slater and G. F. Koster, Phys. Rev. 94, 1498 (1954).
[11]L. P. Bouckaert, R. Smoluchowski, and E. Wigner, Phys. Rev. 50, 58 (1936).
[12]L. F. Mattheiss, Phys. Rev. B 5, 290 (1972).
[13]P. O. Löwdin, J. Chem. Phys. 23, 1833 (1955).
[14]L. F. Mattheiss, Phys. Rev. B 8, 3719 (1973).